OXIDIZED NANO-BACTERIAL CELLULOSE/SILK FIBROIN COMPOSITE FILMS

SHUAIYAN WANG,[*] TAO HUANG,[*] CHEN LAI,[**] TINGFEI XI,[*,**]
SHIBO LIAO[***] and FANG NAN[*]

[*]*School of Laboratory Medicine and Life Science, Wenzhou Medical University,*
Wenzhou 325035, China
[**]*ShenZhen Key Laboratory of Human Tissue Regeneration and Repair, Shenzhen Institute of Peking*
University, Shenzhen 518057, China
[**] *School of Information and Engineering, Wenzhou Medical University, Wenzhou 325035, China*
✉ *Corresponding author: Tingfei Xi, xitingfei@pku.edu.cn*

In this work, we investigate the oxidation reaction conditions for bacterial cellulose and the physical and chemical properties of the resulting composite product. The C6 primary hydroxyls of the bacterial cellulose were selectively oxidized to form carboxylate groups using 2,2,6,6-tetramethyl piperidine-1-oxyl (TEMPO) as a catalyst. The carboxylate content was determined by conductivity titration. The performance of the composite products generated by the oxidation carboxylate cross-linking reactions with the amino acid of silk fibroin was analyzed using the contact angle, surface free energy, FT-IR, and FE-SEM. In the TEMPO/NaClO$_2$/NaClO system, the C6 hydroxyl groups of bacterial cellulose were successfully oxidized, and the optimal conditions were determined. The surface free energy and polarization components of the oxidized bacterial cellulose (OBC) film were found to have increased compared to the pure BC pellicles. The OBC/SF composite film surface free energy was the highest and was more prone to the adsorption of endothelial cells. Based on this work, the OBC/SF composite materials described here demonstrate the potential for use in medical material applications and will provide the basis for further experiments.

Keywords: bacterial cellulose, oxidation, silk fibroin, composite

INTRODUCTION

Bacterial cellulose (BC) is a form of cellulose secreted by organisms such as *Acetobacter* (also known as *Gluconacetobacter*), *Acanthamoeba, Achromobacter and Zoogloea. Acetobacter* is widely studied and exhibits an especially high BC yield, making it suitable for commercial production. The molecular structure of BC is similar to that of plant cellulose and is shown in Figure 1(a). Bacterial cellulose is a linear syndiotactic homopolymer composed of D-anhydroglucopyranose units (AGU), which are linked together by β-1,4-glycosidic bonds. Compared to common plant cellulose, BC has a higher purity, crystallinity and thermal stability (250-300 °C), good biocompatibility[1,2] and water retention capacity,[3] stronger mechanical properties, elastic modulus[4] and plasticity (controllable shaping and a supramolecular structure through

the alteration of the cultivation conditions during fermentation). Its biological functions and applications are based on the unique morphological characteristics of the individual fibers. The individual BC chains aggregate into fibrils, forming ribbons. These ribbons constitute an ultrafine network much finer than plant cellulose fibers. BC has a strong nanofibril architecture resembling collagen, but exhibits no immunological reactivity, and has already been used successfully in biomedical applications. BC can be used to fabricate excellent wound dressings. If BC is compounded with collagen or chitosan, its physical properties are further improved, and it promotes rapid and virtually painless wound healing.[5,6] BC represents an innovative approach to overcoming reconstructive problems in artificial blood vessels associated with extended periods of

vascular disease by providing the ability to perform small diameter vascular grafts.[7] Malm[8] has proven that biosynthetic small caliber vascular grafts made from BC are effective for up to 13 months in sheep carotid arteries. BC is a potential material for use in small caliber grafts, but patency in animal models needs to be improved before clinical studies can be planned. Additionally, artificial bones,[9,10] urethral catheters,[11] skeletal muscles,[12] heart valves[13] and cartilage tissue engineering scaffolds[14,15] are potential avenues for BC. BC has also been used to construct nanofibrous three-dimensional carriers for liver cells,[16] for creating tubes to regenerate damaged peripheral nerves,[17] and for creating carriers for the delivery and differentiation of mesenchymal stem cells[18] and neural stem cells[19] for neural tissue regeneration. However, its compact nanomesh structure may prevent cell migration into scaffolds or sponges composed of it, preventing its use in certain applications.

In recent years, many researchers have attempted to modify BCs physically, chemically or biologically. In most cases, BC modification has focused on improving its applicability and performance in different applications. The C6 primary hydroxyls of bacterial cellulose are selectively oxidized to form carboxylate groups using the TEMPO/NaClO/NaClO$_2$ system.[20-22] The resulting surface of the BC nanofibers is negatively charged and capable of easily combining with other polymers. Peng *et al*. prepared a new type of degradable oxidized bacterial cellulose composite.[23] Multiple patents describing oxidation of BC to create biodegradable BC material are also on file.[24-26]

Silk fibroin (SF) is a natural polymer fibrous protein extracted from silk. SF is composed of 18 α-amino acids, of which Gly, Ala, and Ser are the primary amino acids. Compared to other proteins, the silk fibroin protein is characterized by an Ala-Gly-X primary sequence (see Fig. 1), leading to regular patterns at its primary level.[27] It is biocompatible, biodegradable, non-toxic, and possesses a certain degree of brittleness and oxygen permeability in the wet state.[28] It can be used effectively as a scaffold material and as a coating material for artificial blood vessels. Enomoto *et al*. recently demonstrated that a small caliber graft woven from silk fibroin thread showed good long-term patency. Presently, SF is under study for use in artificial blood vessels.[29,30]

Research has shown that both endothelial cells and smooth muscle cells will migrate into the SF matrix.[31] BC and SF, which are both naturally derived, possess a strong affinity for cells and can provide the approximate extracellular matrix scaffold conditions necessary for growth and development within the body. These conditions can cause the cells to aggregate into the tissue, regulating the structure of the tissue. Therefore, this material has great potential for the fabrication of small blood vessels.

This paper studies the surface structure of the composite film and its surface adsorption. The surface adsorption was determined by calculating the surface free energy based on the contact angle. The morphology of the composite films was observed by field emission scanning electron microscopy (FE-SEM). Fourier transform-infrared (FT-IR) spectroscopy was used to study the conformation of the composite films.

EXPERIMENTAL
Materials
The BC pellicles used in this study were donated by Guangyu Biotechnology Co. Ltd., Chinaand were stored at 4 °C when not in use. TEMPO (AR grade), a NaClO solution (AR grade, 13.4% available chlorine) and NaClO$_2$ (AR grade) were purchased from Sigma-Aldrich (USA) and used unpurified. The silk fibroin powder (92% or higher purity) was purchased from Hubei Blue Sky Manufacturing Co. Ltd., China.

Oxidation of BC pellicles
The bacterial cellulose pellicles in a hydrogel state were extracted from deionized water and immersed in a 0.25 M aqueous sodium hydroxide solution for 48 h at room temperature before being repeatedly washed with deionized water until the pH of the solution reached 7. Filter paper was used to remove excess water from the surface, which contained tailored pellicles with a size of 4 cm × 4 cm and a thickness 1 mm. The pellicles were suspended in a 0.05 M phosphate buffer solution (100 ml, pH = 6.86). TEMPO, NaClO$_2$ and NaClO were added to the solution until the concentration of the NaClO was diluted to 0.1 M. The same 0.05 M buffer was used as oxidization medium. The suspension was stirred at approximately 60 °C to initiate the reaction. Additionally, both the reaction starting and ending times were recorded.

Determination of carboxylate content of bacterial cellulose films
The carboxylate content of the oxidized BC films was determined using the electric conductivity titration method.[32] After being washed and freeze-dried, the oxidized BC films were suspended in water (80 ml) and

stirred. After 0.01 M NaCl (5 ml) was added, the pH value of the suspension was adjusted to a range from 2.5 to 3.0 using 0.1 M HCl. Conductometric titration was performed using a TitraLab TIM854 (Hach, USA) with 0.04 M NaOH as titrating solution. The carboxyl group content is determined from the following equation (1):

$$n_{COOH} = \frac{(V_2 - V_1)C}{S} \tag{1}$$

where V_2 and V_1 are the inflection points in the titration curve corresponding to the amount of consumed NaOH, C is the NaOH concentration (mole per liter), and S is the area of the OBC.

Composite films

The silk fibroin solution was prepared by dissolving the silk fibroin powder in deionized water and heating until a transparent, golden liquid formed, yielding a 10% (w/v) solution. The composite films were prepared by adding 25 ml of the aqueous silk fibroin solution to the oxidized bacterial cellulose pellicles at room temperature for several days, followed by drying 37 °C for about 4 h in a vacuum oven.
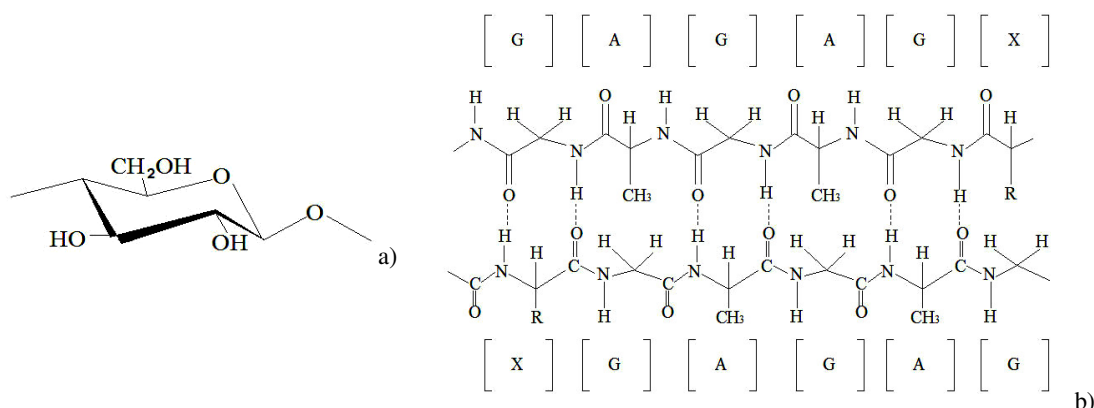

Figure 1: Molecular structures of (a) bacterial cellulose and (b) silk fibroin

Material characterization

Determination of contact angle and surface free energy

The water and glycerin contact angles were measured with an OCA20 data physics instrument (Data Physics, Germany), using the sessile drop technique. The pure BC, OBC, BC/SF and OBC/SF were individually mounted on glass slides using double-sided adhesive tape. The contact angle tests were conducted at eight different positions at the film surface. Each recorded value was an average of eight different measurements. The polar and dispersive components of the BC surface energy were calculated using the Owens–Wendt approach.

FT-IR spectrometry

ATR-FTIR spectroscopy of the sample films was performed using a Nicolet 6700 spectrometer (Thermo, USA) with a resolution of 4 cm^{-1} over a range of 400 to 4000 cm^{-1}. The silk fibroin solution was processed using the same method.

FE-SEM

The network structure of the BC and the surface of the composite films were observed using SEM (MIRA3 TESCAN, Czech Republic).

RESULTS AND DISCUSSION

Determination of the oxidation process for the bacterial cellulose films

The C6 primary hydroxyl groups in the bacterial cellulose were selectively oxidized to form carboxylate groups using the TEMPO/NaClO/NaClO$_2$ system (see Fig. 2). In the oxidation system, the degree of oxidation of the cellulose C6 was the highest when carried out at pH 6.8 and at a temperature of 60 °C.[33] For constant conditions, the carboxylate content increased with the reaction time before reaching a plateau after 40 h (see Fig. 3). However, Saito[33] showed that the pH and temperature did not change, and after a reaction time of 24 h, the carboxyl content was essentially unchanged. In this experiment, broken wood pulp was oxidized to form the BC pellicles. As a result of the initially different states of the reactants, the films were effectively the same density. Therefore, more time was required for the C6–OH molecular structure to form from the oxidant and catalyst reaction. Compared with other natural cellulose materials,

BC has a highly compact structure, which serves to impede the reaction rate.[34]

BC films oxidized by the TEMPO/NaClO/NaClO$_2$ system were also investigated to clarify the effect of increasing the amount of TEMPO on the carboxylate content of the oxidized BC (see Fig. 4). Using TEMPO as a catalyst greatly accelerated the reaction rate, but had no effect on the oxidation yield. In other words, the carboxylate content of the oxidized BC films was constant. This is likely because the amount of NaClO$_2$ oxidant was inadequate or the reaction time was not sufficient. When the concentration of the TEMPO was 0.3 mmol/L, the carboxylate content reached approximately 220 mmol/m^2 for 10 h. When the other conditions were consistent and the amount of TEMPO was 0.1 mmol/L, the carboxyl content reached more than 200 mmol/m^2 for nearly 40 h (Fig. 3). From this result, it was obvious that the reaction time substantially decreased. Therefore, the reaction process is accelerated by increasing the quantity of the catalyst available to the reaction.

When the concentrations of the TEMPO, NaClO and NaClO$_2$ were 0.1 mmol/ L, the carboxylate content was approximately 115 mmol/m^2 for a reaction time of 10 h, as shown in Figure 4. The effect of adding NaClO was also studied. In Figure 5, the carboxylate content of the BC oxidized at pH 6.8 and a temperature of 60 °C for 10 h was plotted versus the amount of NaClO added. The activity of the catalyst did not plateau, so the reaction was accelerated by increasing the amount of the co-catalyst. However, the carboxyl content of the oxidation reaction remained constant. As seen from the plot, the initial portion of the curve shows a fast reaction, followed by a slower period. The turning point at 0.4 mol/L NaClO was the most appropriate operating point, because excessive NaClO has a negative effect on the BC films.
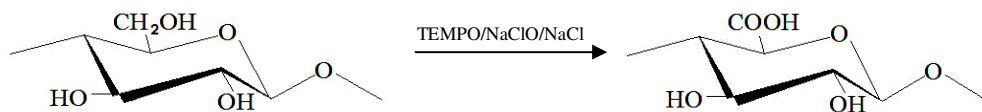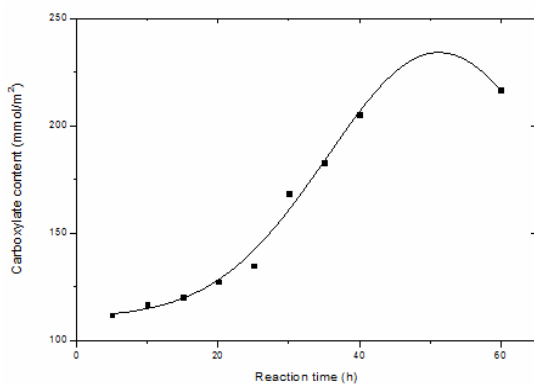

Figure 2: Oxidation process for the BC film

Figure 3: Effect of additional reaction time on the oxidation of the BC film (100 ml 0.05 M PBS, 0.0016 g TEMPO, 0.5 ml 2 M NaClO, 0.5 g NaClO$_2$; system conditions include pH 6.8, a temperature of 60 °C, and a reaction time of 10 h)
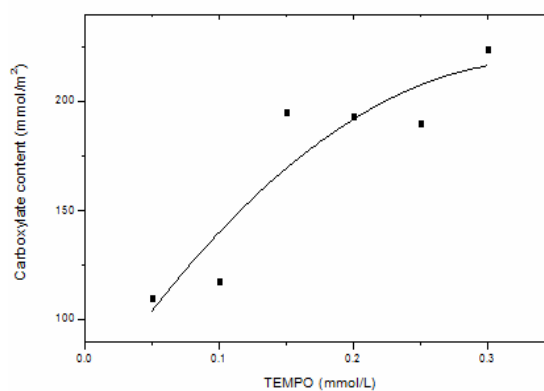
Figure 4: Effect of TEMPO addition on the oxidation of the BC film (100 ml 0.05 M PBS, 0.5 ml 2 M NaClO, 0.5 g NaClO$_2$; system conditions include pH 6.8, a temperature of 60 °C, and a reaction time of 10 h)
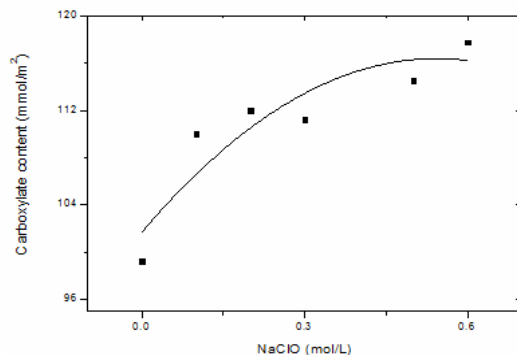
Figure 5: Effect of NaClO addition on the oxidation of the BC film (100 ml 0.05 M PBS, 0.0016 g TEMPO, 0.5 g NaClO$_2$; system conditions include pH 6.8, a temperature of 60 °C, and a reaction time of 10 h)

Table 1
Contact angle and surface free energy

	Contact angle		$\gamma_S^d + \gamma_S^p$	γ_S^d	γ_S^p	FP
	Water	Glycerol	(mN/m)	(mN/m)	(mN/m)	$\gamma_S^p/(\gamma_S^d + \gamma_S^p)$
1	36.94	42.19	69.03	5.17	63.33	0.92
2	36.59	47.29	80.06	1.74	78.32	0.98
3	45.4	50.03	62.32	4.81	57.51	0.92
4	38.39	58.95	115.14	1.1	114.04	0.99

Note: 1 (BC), 2 (OBC), 3 (BC/SF), 4 (OBC/SF)

Characteristics of oxidized nano-bacterial cellulose/silk fibroin composite films
Contact angle and surface free energy analysis

The contact angles, dispersion and polar surface tension components, fractional polarity (FP), and surface energy of the different materials are shown in Table 1. The BC, OBC, BC/SF, and OBC/SF are hydrophilic materials because their contact angles are smaller than 90°; the smaller the contact angle, the greater the hydrophilicity of the material. Compared with the pure BC film, the surface free energy and the polar components of the OBC film increased. This increase is the result of the surface hydroxyl groups being substituted by more polar carboxylate groups. The surface free energy of the OBC/SF was determined to be the greatest, as shown in Table 1. The interaction of the dispersion force and the polarity force between the solid and liquid states and the solid surface free energy can be represented by:

$$\gamma_S = \gamma_S^d + \gamma_S^p \qquad (2)$$

where γ_S^p are the polar components that include the interactions of the dipole and the hydrogen bonding.

The value of this variable is influenced by the surface polar factors γ_S^d. The dispersive components include the interactions between nonpolar molecules and are influenced by the density. Of the two surface energy components, the polar component γ_S^p appears to be the most accurate at predicting the cellular adhesion strength. This is the result of a causal relationship between the polar surface energy and the cellular adhesion strength. The fractional polarity, $\gamma_S^p/(\gamma_S^d + \gamma_S^p)$, which has been previously correlated to cell spreading and growth (defined by some as a measure of the cellular adhesion)[35,36] demonstrated a roughly parabolic relationship with the cellular adhesion strength.[37] Hallab et al.[37,38] proposed an 'S' curve schematic relationship between surface energy and cellular adhesion strength. Therefore, the material's surface adsorption was observed to be the strongest under certain conditions, which provides evidence for the adsorption trials of the endothelial cells in the next step. The ability of directed cell responses to material surfaces is dependent on the surface characteristics of the biomaterials that affect the implant cell interactions. Olivares-Navarrete[39] determined that the surface free energy of a substrate plays a role in regulating bone cell responsiveness. Therefore, the surface free energy may be an important determinant in cell adhesion to and proliferation on

FT-IR analysis

FT-IR spectroscopy measurements were performed to investigate the conformational characteristics of the films. As shown in Figure 6, pure BC (a) exhibits wide absorption bands at 3350 cm^{-1}, which are attributed to O-H stretching vibrations. However, for the BC/SF (d) films, the peak shifted to a lower wavenumber. This is the result of the increasing number of intermolecular hydrogen bonds due to the introduction of protein into the cellulose.[40] The distinct characteristic absorption peaks of the BC at 1060 cm^{-1} is attributed to C-O-C stretching vibrations. The peak at 2895 cm^{-1} corresponds to the C-H stretching vibrations of aliphatic hydrocarbons. After the TEMPO oxidation occurred (-CH₂OH changed -COOH), a wider peak appeared at 3400~2200 cm^{-1} than that for pure BC, which was attributed to the dispersive absorption band of -OH stretching vibrations in carboxylic acid. After compounding with SF, the spectral region 3400~2450 cm^{-1} included N-H stretching vibrations. This is a characteristic of asymmetric C=O stretching vibrations in the COO− group located at 1620~1540 cm^{-1}. In Figure 6, the carbonyl group C=O stretching vibrations associated with carboxylic acid are seen at 1760~1660 cm^{-1}. Therefore, the strong absorption peak that appeared at 1636 cm^{-1} could be formed by a fusion of two peaks, indicating the successful oxidation of the hydroxyl groups.
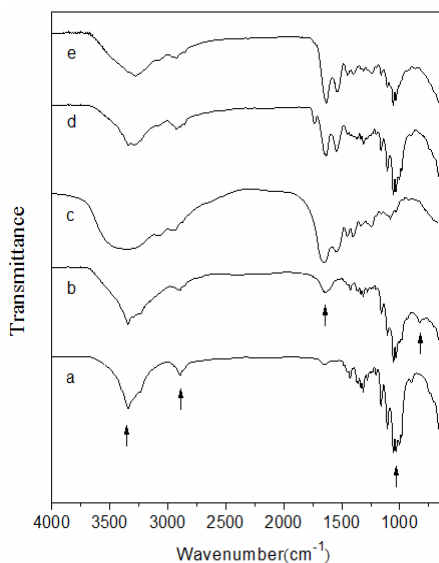

Figure 6: FTIR spectra of the blended film over a range of 4000~650 cm^{-1}: (a) BC, (b) OBC, (c) SF, (d) BC/SF, (e) OBC/SF
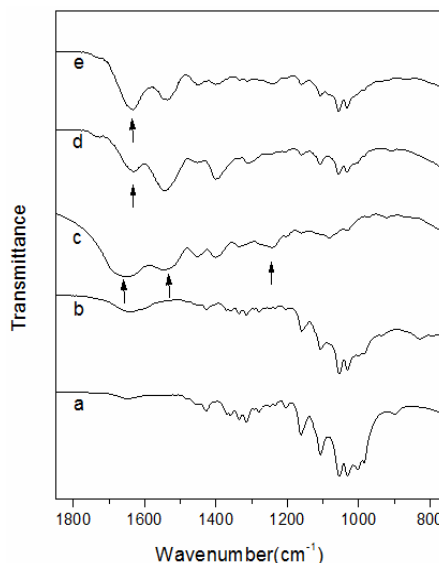

Figure 7: FTIR spectra of the blended film over a range of 1850~750 cm^{-1}: (a) BC, (b) OBC, (c) SF, (d) BC/SF, (e) OBC/SF
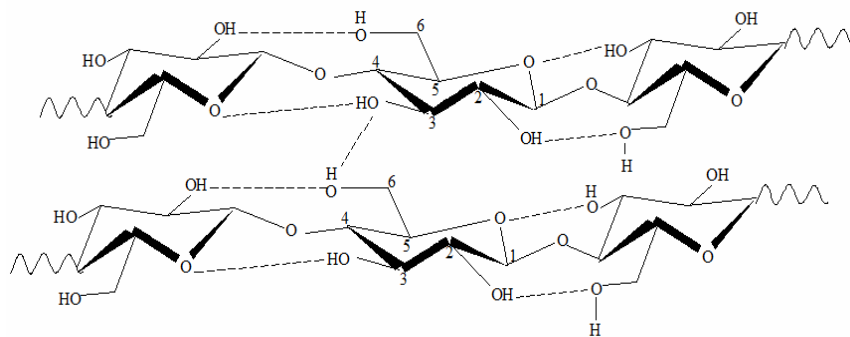

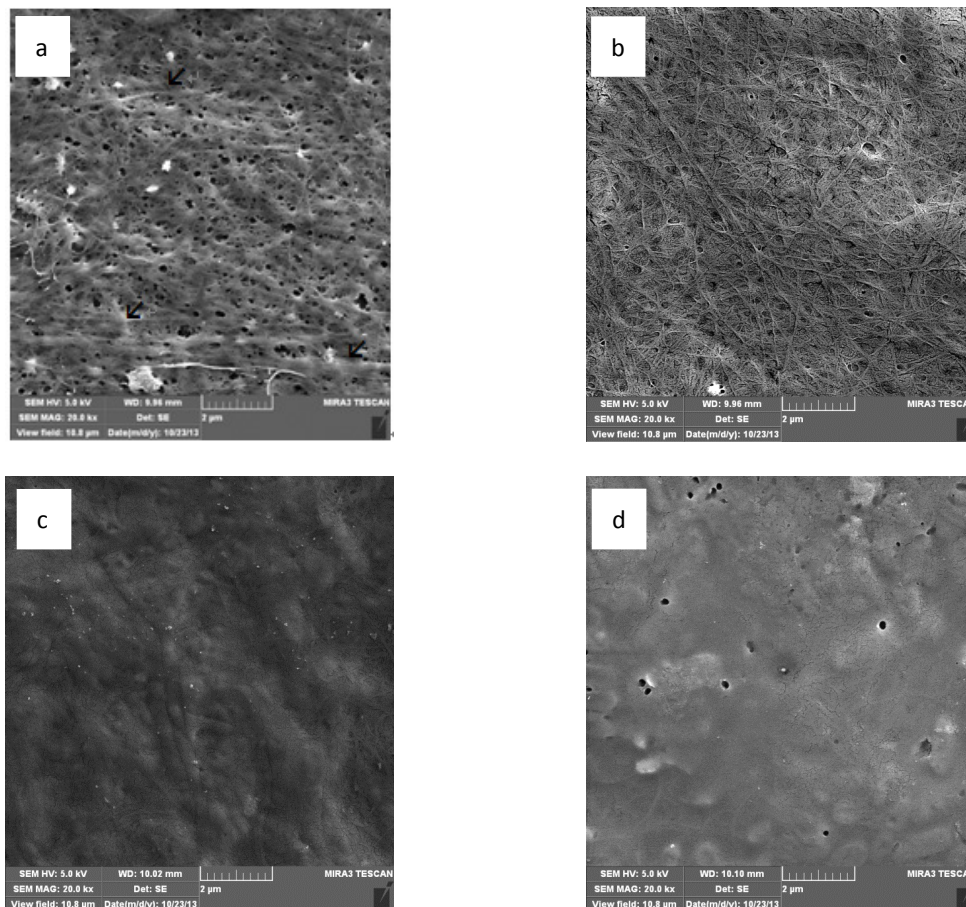Figure 8: Intra- and inter-molecular hydrogen bonds in the BC

Figure 9: SEM images of the surfaces of (a) BC, (b) OBC, (c) BC/SF, (d) OBC/SF

The OBC peak at 890 cm^{-1} is the characteristic absorption peak of the oxidized fiber[41] and is assigned to the hemiacetal bonds between the aldehyde groups and the hydroxyl groups. The characteristic absorption bands of the silk fibroin at 1630 cm^{-1} (amide I), 1530 cm^{-1} (amide II) and 1260 cm^{-1} (amide III) are assigned to the crystalline β-sheet structure, whereas the bands at 1660 cm^{-1} (amide I), 1540 cm^{-1} (amide II) and 1230 cm^{-1} (amide III) are attributed to the random coil form or silk.[42] In Figure 7(c), the C=O peaks from the protein amide stretching occurred at 1656 cm^{-1} (amide I), 1545 cm^{-1} (amide II), and 1246 cm^{-1} (amide III). This is indicative of random coils or the silk conformation of the SF. When forming the BC/SF or OBC/SF composite films, the amide bands of the SF were shifted slightly to 1633 cm^{-1}. This result illustrates that the strong interactions between the SF and either the BC or the OBC induced the conformational transition of the SF from a random coil form or silk I to a β-sheet structure.[43] Due to the crystalline β-sheet structure of the composite films, these materials were insoluble in water.[44] The OBC and BC had similar influences on the structure of the SF. The weakened peak at 1240 cm^{-1} was assigned to the secondary amide C-N stretching vibrations and the amide bands that were formed through the –COOH of the OBC and the -NH$_2$ of the SF.

FE-SEM analysis

As seen in Figure 9(a), the surfaces of the BC consisted of a mutual crisscross mesh structure with randomly entangled ribbons. The arrows indicate the agglomerations of the nanofibers. There are many hydroxyl groups in BC that exhibit a strong tendency to form intra- and inter-molecular hydrogen bonds (Fig. 8). These cause the fibers to tightly entangle. As a result of these fibers alternating in bunches and forming clusters, the distribution was uneven and gave the appearance of a heterogeneous aperture. The

texture of oxidized BC was clearer and more evenly distributed, and the fiber mesh was looser than that seen in naturally occurring BC. The individual cellulose nanofibers are clearly observed in Figure 9(b). The reason is that the intra- and inter-molecular hydrogen bonds were disrupted on the BC surface because the C6 primary hydroxyl groups of the BC were oxidized to form carboxylate groups. Meanwhile, the OBC nanofibers were negatively charged. The increased surface charge density of the fibers improved the fiber dispersion due to the increased charge repulsion, which decreased the fiber entanglement.[41] From Figure 9(c) and (d), it is seen that the individual cellulose fibrils were coated with silk fibroin. In the composite films, the cellulose and SF possessed good compatibility, which was the result of strong hydrogen bonding between the hydroxyl groups of the cellulose and amino groups of the SF. The surface of the OBC/SF was slightly smoother than the surface of

the BC/SF. The surfaces of BC/SF particles were formed by combining BC with SF through non-covalent bonding, including hydrogen bonds and hydrophobic keys. The SF molecules aggregated unevenly on the BC membranes so that the surfaces of the composite films were seen to sag and crest (see Fig. 10). Brown *et al.*[45] also confirmed that the silk fibroin penetrated well into the fibrous structure of the BC. The OBC combined with the SF through covalent bonds, which are stronger than hydrogen bonds, occur quicker, and are more ordered. When the oxidized cellulose was treated with the SF solution, the resulting surface was smooth again. This illustrates that the SF treatment can modify the surface properties of the cellulose, especially the oxidized cellulose.[46] Therefore, this method can be attempted in adsorption trials on endothelial cells to observe their proliferation and differentiation on the surface.
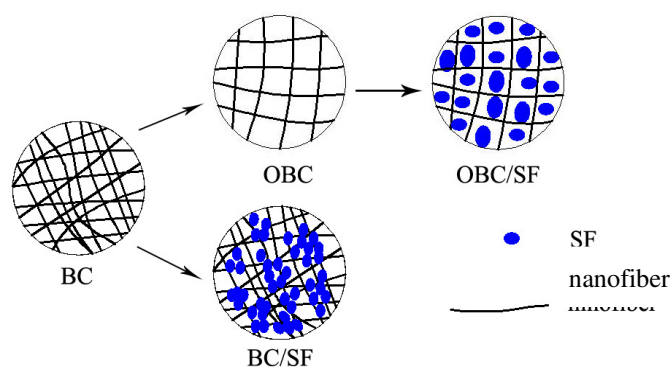

Figure 10: Schematic illustration of BC/SF and OBC/SF composite films

CONCLUSION

In this work, the C6 region of BC has been successfully oxidized using a TEMPO/NaClO$_2$/NaClO system, so that the primary hydroxyl groups were converted to form carboxylate groups. The conversion makes it possible to reduce the adhesion between the cellulose fibrils by preventing the formation of strong inter-fiber hydrogen bonds. The SF is bonded to the oxidized bacterial cellulose films, resulting in the secondary structure of the SF changing from random coils or silk structures into β-sheet structures. The crystallinity also changes. These composite films are water resistant. In

addition, introducing large amounts of carboxylate groups at the surface of the BC fibers led to an increase in the surface free energy, especially for the polar components. The surface morphologies of the BC are significantly different before and after the oxidation and were studied using SEM. As the reactions proceed, the internal structure becomes less compact. The reasons for this are that the hydrogen bonds between the nanofibers are destroyed and that the surface of cellulose nanofibers is negatively charged through the introduction of carboxylate groups during the oxidation reaction. This surface modification provides a promising method for modifying BC to

satisfy the technical needs of a large variety of applications. At present, there have been many studies on the preparation of medical dressings using bacterial cellulose. However, the studies on the preparation of artificial blood vessels and bones are limited to testing for physical and chemical properties and animal experiments. Clinical applications are still in the initial stages. With further research, biological materials will be able to satisfy the basic requirements for blood vessels in the human body. These naturally originating polymer-based materials offer advantages, such as the creation of new opportunities for mimicking tissue micro-environments and stimulating the appropriate physiological responses required for cellular regeneration.[47] Natural biological materials are easy to introduce after the adsorption of cells. There is an increasing need for vascular grafts in the field of surgical revascularization, which may be met using BC fabricated blood vessels. Other applications for modified bacterial cellulose will likely focus on high value added biomedical materials. We aimed at investigating the use of fibroin and bacterial cellulose-based nanomaterials as a cellular vascular graft for *in vivo* recellularization.

REFERENCES
[1] F. G. Torres, S. Commeaux and O. P. Troncoso, *J. Funct. Biomater.*, **3**, 864 (2012).
[2] N. Petersen and P. Gatenholm, *Appl. Microbiol. Biotechnol.*, **91**, 1277 (2011).
[3] C. Fitz-Binder and T. Bechtold, *Carbohyd. Polym.*, **106**, 142 (2014).
[4] A. Retegi, I. Algar, L. Martin, F. Altuna and P. Stefani *et al.*, *Cellulose*, **19**, 103 (2012).
[5] C. Wiegand, P. Elsner and U. C. Hiple, *Cellulose*, **13**, 689 (2006).
[6] D. Ciechanska, *Fibres Text.*, **12**, 69 (2004).
[7] D. A. Schumann, J. Wippermann, D. O. Klemm, F. Kramer, D. Koth *et al.*, *Cellulose*, **16**, 877 (2009).
[8] C. J. Malm, B. Risberg, A. Bodin, H. Bäckdahl, B. R. Johansson *et al.*, *Scand. Cardiovasc. J.*, **46**, 57 (2012).
[9] S. A. Hutchens, R.S. Benson, B. R. Evans, H. M. O'Neill, C. J. Rawn *et al.*, *Biomaterials*, **27**, 4661 (2006).
[10] Q. Shi, Y. Li, J. Sun, H. Zhang, L. Chen *et al.*, *Biomaterials*, **33**, 6644 (2012).
[11] A. Bodin, S. Bharadwaj, S. Wu, P. Gatenholm, A. Atala *et al.*, *Biomaterials*, **31**, 8889 (2010).
[12] J. M. Dugan, R. F. Collins, J. E. Gough and S. J. Eichhorn, *Acta Biomater.*, **9**, 4707 (2013).
[13] H. Mohammadi, *Proc. Inst. Mech. Eng. H*, **225**, 718 (2011).
[14] A. Svensson, E. Nicklasson, T. Harrah, B. Panilaitis, D. L. Kaplan *et al.*, *Biomaterials*, **26**, 419 (2005).
[15] J. Andersson, H. Stenhamre, H. Bäckdahl and P. Gatenholm, *J. Biomed. Mater. Res. A*, **94**, 1124 (2010).
[16] M. Bhattacharya, M. M. Malinen, P. Lauren, Y. R. Lou, S.W. Kuisma *et al.*, *J. Control. Release.*, **164**, 291 (2012).
[17] K. Kowalska-Ludwicka, J. Cala, B. Grobelski, D. Sygut, D. Jesionek-Kupnicka *et al.*, *Arch. Med. Sci.*, **9**, 527 (2013).
[18] H. Gu, Z. Yue, W. S. Leong, B. Nugraha and L. P. Tan, *Regen. Med.*, **5**, 245 (2010).
[19] A. J. Mothe, R. Y. Tam, T. Zahir, C. H. Tator and M. S. Shoichet, *Biomaterials*, **34**, 3775 (2013).
[20] T. Saito and A. Isogai, *Biomacromolecules*, **5**, 1983 (2004).
[21] T. Saito, I. Shibata, A. Isogai, N. Sguri and N. Sumikawa, *Carbohyd. Polym.*, **61**, 414 (2005).
[22] T. Saito, Y. Okita, T. T. Nge, J. Sugiyama and A. Isogai, *Carbohyd. Polym.*, **65**, 435 (2006).
[23] S. Peng, Y. Zheng, J. Wu, Y. Wu, Y. Ma *et al.*, *Polym. Bull.*, **68**, 415 (2012).
[24] V. Kumar and Y. Dang, US Patent 20107662801, 2010.
[25] J. Harris, G. Serafica, C. Damien and H. Nonnenmann, US Patent 20107709631, 2010.
[26] L. Saferstein, G. Serafica, US Patent 20107645874, 2010.
[27] C. Vepari and D. L. Kaplan, *Prog. Polym. Sci.*, **32**, 991 (2007).
[28] K. Inouye, M. Kurokawa, S. Nishikawa and M. Tsukada, *J. Biochem. Biophys. Meth.*, **37**, 159 (1998).
[29] I. Cattaneo, M. Figliuzzi, N. Azzollini, V. Catto, S. Farè *et al.*, *Int. J. Artif. Organs*, **36**, 166 (2013).
[30] X. Y. Yang, L. Wang, G. P. Guan, M. W. King, Y. L. Li *et al.*, *J. Biomater. Appl.*, **27**, 1 (2012).
[31] S. Enomoto, M. Sumi, K. Kajimoto, Y. Nakazawa, R. Takahashi *et al.*, *J. Vasc. Surg.*, **51**, 155 (2010).
[32] K. Tôei and T. Kohara, *Anal. Chim. Acta*, **83**, 59 (1976).
[33] T. Saito, M. Hirota, N. Tamura and A. Isogai, *J. Wood Sci.*, **56**, 227 (2010).
[34] C. Lai, S. J. Zhang, L. Y. Sheng, S. B. Liao, T. F. Xi *et al.*, *Colloid. Polym. Sci.*, **291**, 2985 (2013).
[35] J. M. Schakenraad, H. J. Busscher, C. R. Wildevuur and J. Arends, *J. Biomed. Mater. Res.*, **20**, 773 (1986).
[36] R. D. Bagnall, J. A. Annis and S. J. Sherliker, *J. Biomed. Mater. Res.*, **18**, 1 (1980).
[37] N. Hallab, K. Bundy, O. Kim, R. Moses and J.

Jacobs, *Tissue Eng*., **7**, 55 (2001).

[38] P. van der Valk, A. W. J. van Pelt, H. J. Busscher, H. P. de Jong, Ch. R. H. Wildevuur *et al*., *J. Biomed. Mater. Res*., **17**, 807 (1983).

[39] R. Olivares-Navarrete, A. L. Raines, S. L. Hyzy, J. H. Park, D. L. Hutton *et al*., *J. Bone Miner. Res*., **27**, 1773 (2012).

[40] G. Yang, L. Zhang and Y. Liu, *J. Membrane Sci*., **177**, 153 (2000).

[41] H. Liimatainen, M. Visanko, J. A. Sirviö, O. E. O. Hormi and J. Niinimaki, *Biomacromolecules*, **13**, 1592 (2012).

[42] G. Freddi, M. Romano and M. Rosaria, *J. Appl. Polym. Sci*., **56**, 1537 (1995).

[43] S. Shang, L. Zhu and J. Fan, *Carbohyd. Polym*., **86**, 462 (2011).

[44] R. Jung and H. J. Jin, *Key Eng. Mater*., **342-343**, 741 (2007).

[45] E. Brown, J. W. Zhang and M. Laborie, *Cellulose*, **18**, 631 (2011).

[46] H. Lin, L. R. Yao, Y. Y. Chen and H. Wang, *Fiber. Polym*., **9**, 113 (2008).

[47] S. S. Silva, J. F. Mano and R. L. Reis, *Crit. Rev. Biotechnol*., **30**, 200 (2010).